Appl Phys B (2009) 94: 467–471
DOI 10.1007/s00340-008-3327-5

Applied Physics B
Lasers and Optics

Photorefractive properties of optical waveguides in Fe:$LiNbO_3$ crystals produced by O^{3+} ion implantation

Y. Tan · F. Chen · D. Kip

Received: 26 August 2008 / Revised version: 11 November 2008 / Published online: 11 December 2008

Abstract The photorefractive properties of optical planar waveguides in Fe:$LiNbO_3$ crystals fabricated by O^{3+} ion implantation are investigated. Two-wave mixing experiments are carried out for both the waveguide and the bulk. The results show that the measured gain coefficients are almost identical for the waveguiding layer and the substrate. In the waveguide, the response time could be reduced by one order of magnitude, with respect to the bulk, at the same power level of the incident light.

PACS 42.82.Et · 61.80.Jh · 42.70.Nq

1 Introduction

Photorefractive (PR) materials, in which rather large light-induced refractive index changes can be obtained at low optical power levels, have attracted great attention for their potential applications in holographic storage and optical communications [1–3]. Waveguides, as the basic components for integrated photonics, confine light in very small volumes, with transverse dimensions of the order of micrometers [4]. Consequently, many properties of the substrate materials can be considerably improved through waveguide structures because of their higher optical intensities compared to bulk materials [4–8], which leads, in general, to much faster response times. In addition, such compact configurations could make waveguide devices easily connectable with optical fibers that have been widely applied in modern telecommunications [9]. Therefore, PR waveguides received considerable attention due to the combination of micro-sized dimensions and abilities to tailor refractive index changes, which could be used for many photonic applications, such as optical phase conjugation, optical switches/interconnections, and reflection filters [5, 10–13].

Lithium niobate ($LiNbO_3$) crystals are well known for excellent performance in electro-optical, nonlinear optical, and acousto-optical applications [14]. When doped with metal ions, e.g., Fe or Cu, large PR index changes can be obtained in this material [1, 5, 15]. Usually two well established techniques were applied to fabricate optical waveguides in $LiNbO_3$ crystals, metal-ion in-diffusion using, e.g., titanium (Ti) or zinc (Zn) [16, 17], and proton exchange [18] (or annealed proton exchange [19]). Recently, ion implantation has been proved to be a successful method to form waveguide structures in numerous optical materials, including crystals, glasses, semiconductors, and organic materials [20–29]. Ion-implanted waveguides in $LiNbO_3$ have been realized by using ions of both light species (e.g., H or He) [20, 22] and heavy elements (e.g., C, O, Cl, etc.) [23–25] for multiple applications, such as second harmonic generation [26], laser operation [27], and photonic gratings [28]. The PR properties of He-implanted $LiNbO_3$ waveguides have been investigated by two-wave mixing (TWM) [29], whilst there is no report on related light-induced effects in heavy-ion-implanted $LiNbO_3$

Y. Tan · F. Chen (✉)
School of Physics, Shandong University, Jinan 250100, China
e-mail: drfchen@sdu.edu.cn
Fax: +86-531-88565167

F. Chen
State Key Laboratory of Crystal Materials, Shandong University, Jinan 250100, China

D. Kip
Institute of Physics and Physical Technologies, Clausthal University of Technology, 38678 Clausthal-Zellerfeld, Germany

waveguides. In this work, we report on planar waveguides in Fe:$LiNbO_3$ produced by 6 MeV oxygen ion implantation, and investigate the PR effects in both the waveguiding layer and the substrate using the TWM technique.

2 Experiments in details

The x-cut Fe:$LiNbO_3$ samples used in this work are doped with 0.1 mol% Fe, and cut to pieces with dimensions of $2(x) \times 5(y) \times 10(z)$ mm^3 (the z-axis points along the c-direction of the crystal). The samples are oxidized in pure O_2 atmosphere at 1000°C for several hours, in order to increase the concentration $c_{Fe^{3+}}$ of filled electron traps. One optically polished facet (with size of 5×10 mm^2) of the wafer is implanted by O^{3+} ions at an energy of 6 MeV and a dose of 2×10^{14} ions/cm^2 at room temperature, using the 2×1.7 MV tandem accelerator at Peking University, China. The beam direction is set to be titled 7° off the normal plane of the sample surface in order to minimize channeling effects during implantation. After the implantation, the samples are annealed at 260°C for 30 min in air. Finally, input and output facets (with sizes of 2×5 mm^2) are polished to allow for coupling light into and out of the sample.

Transmission spectra are measured by a spectrophotometer (Jasco U570, China, with resolution of 1 nm) for the as-implanted and annealed samples to investigate possible modifications of surface absorption due to annealing effects. The guiding properties (dark mode spectra) of the waveguide are characterized by the well-known m-line method [30] (linearly polarized He–Ne laser, wavelength 632.8 nm) by using a prism coupler (Metricon Model 2010 with a rutile prism, refractive index resolution of $\pm 2 \times 10^{-4}$). Propagation loss of the sample is determined by measuring scattered light intensity on top of the waveguiding layer versus propagation length.

Figure 1 shows a schematic plot of the TWM experiment. An extraordinarily polarized light beam from a He–Ne laser at wavelength 632.8 nm is split into two parts, through a beam splitter, to form the signal and pump beams, respectively. An attenuator is used to control the power of the signal beam. Both two beams are passing through a cylindrical lens, in order to minimize the light broadening due to the diffraction, and focused by a 20× microscope objective (NA = 0.65). The focused beams are coupled into the waveguide, and out-coupled by another 10× microscope objective (NA = 0.3). A powermeter is used to periodically measure the output light powers of the two beams through a chopper.

3 Results and discussion

In Fig. 2, a comparison of the transmission spectra in the wavelength range 300–800 nm for the as-implanted and annealed sample are given. As one can see, after annealing the

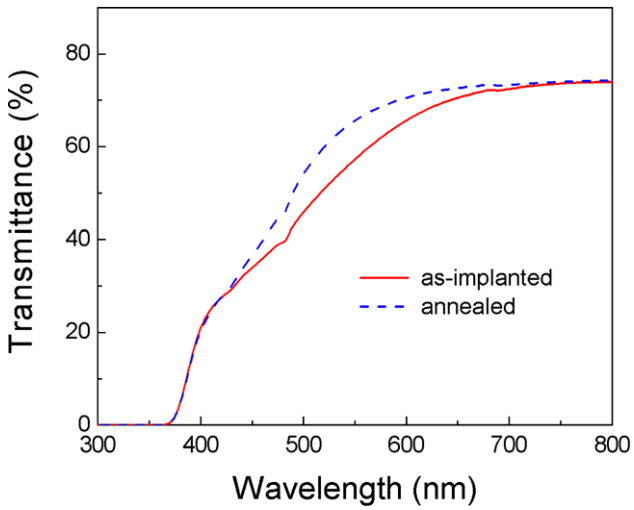

Fig. 2 A comparison of transmission spectra for the as-implanted and annealed (at 260°C for 30 min in air) Fe:$LiNbO_3$ samples

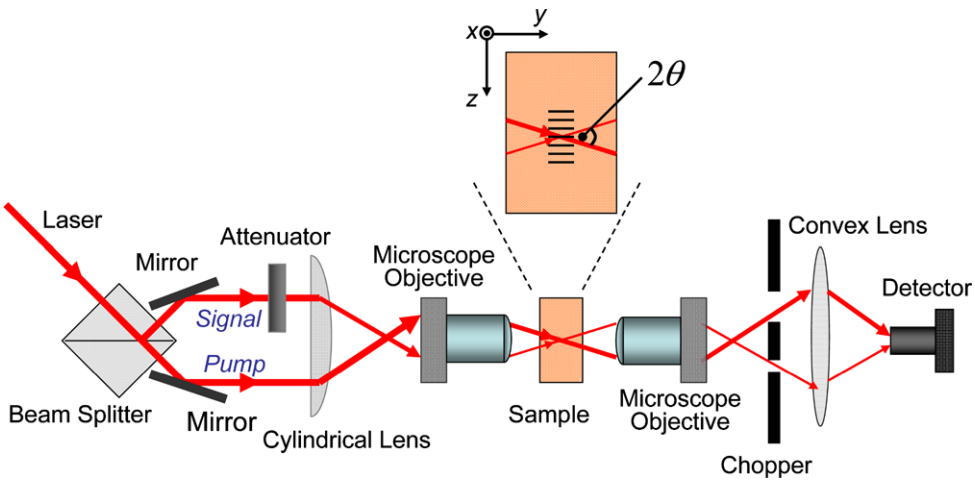

Fig. 1 A schematic plot of experimental TWM setup and crystal configuration. Here the full intersection angle $2\theta \approx 16°$ is measured inside the waveguide

transmittance of the sample is significantly enhanced. Obviously, implantation-induced color centers, which mainly contribute to the additional damping of visible light in the waveguiding layer in the as-implanted sample, can be removed by the performed annealing treatment, thus reducing the induced disorder in the lattice.

Figure 3 depicts the dark mode spectra for both transverse electric (TE) and transverse magnetic (TM) modes of the waveguide at the wavelength of 632.8 nm. Here the TE and TM polarizations correspond to the extraordinary (n_e) and ordinary (n_o) refractive index of the crystal. It should be noted that the first (fundamental) TE_0 has a higher effective refractive index n_{eff} than the substrate value $n_{e,sub}$, which results from an enhanced index well formed in the implanted waveguide region due to electronic damage [24]. On the other hand, all TM modes have a lower n_{eff} than the bulk value $n_{o,sub}$. We reconstruct the index profiles of both n_e and n_o of the waveguide through a computer code based on the reflectivity calculation method (RCM) [31], see Fig. 4. As one can see, the profile of n_e has the expected "well+barrier" distribution whilst the n_o profile is of the typical "barrier" type. In both cases, the barrier depth of ~3 μm coincides with the calculated end-of-range (nuclear) damage peak obtained by TRIM simulation. Low propagation loss of ~0.5 dB/cm for the TE mode is obtained, which is mainly due to the non-leaky confinement of the extraordinarily polarized light. On the other hand, no transmission of light of TM modes is observed from the output facet of the waveguide, which is usually due to the poor light confinement of such "barrier" type n_o profile. Therefore, the O^{3+} ion-implanted Fe:$LiNbO_3$ waveguide guides only n_e polarized light.

The dependence of incident beam power ratio β_0 on the TWM gain factor γ_0 at wavelength of 632.8 nm is monitored in Fig. 5 for both the waveguide and the bulk crystal. Here β_0 and γ_0 are defined as follows [1]:

$$\beta_0 = \frac{P_s}{P_p}, \tag{1}$$

$$\gamma_0 = \frac{I_s \text{ (with pump)}}{I_s \text{ (without pump)}}, \tag{2}$$

where P_s and P_p are the powers of signal and pump beam in the waveguide and the bulk, respectively. The values P_s and P_p inside the sample are obtained by measuring the out-coupled power, corrected by Fresnel losses inside the crys-

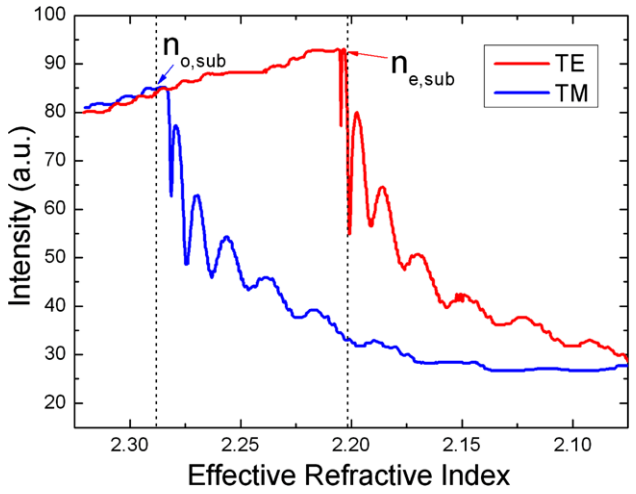

Fig. 3 Dark mode spectra of TE and TM modes for the O^{3+} implanted waveguide in Fe:$LiNbO_3$ after annealing at 260°C for 30 min. *Vertical dotted lines* show the position of ordinary and extraordinary bulk indices

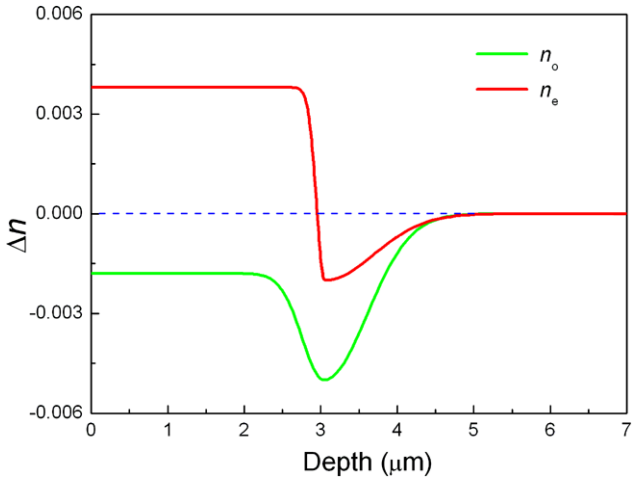

Fig. 4 Refractive index (n_o, *green line*; n_e, *red line*) profiles of the O^{3+} implanted waveguide in Fe:$LiNbO_3$ after annealing at 260°C for 30 min

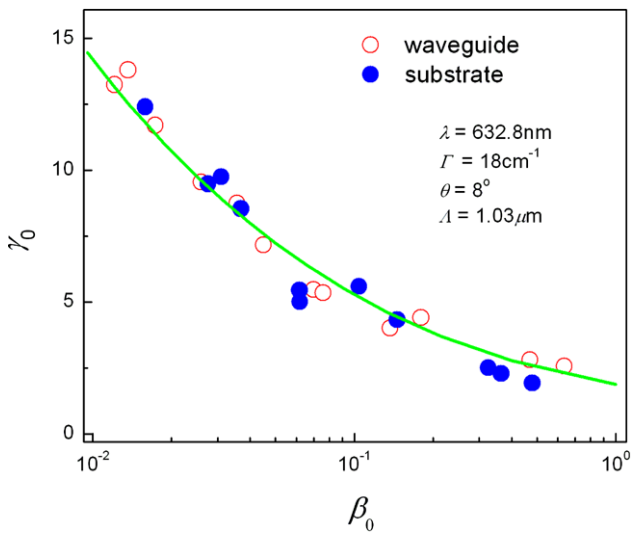

Fig. 5 TWM gain γ_0 as a function of beam power ratio β_0 measured at a wavelength of $\lambda = 632.8$ nm in the waveguide (*open circles*) and bulk (*filled circles*). The intersection angle inside the sample is $2\theta \approx 16°$, and the grating spacing is $\Lambda = 1.03$ μm. A numerical fit (*solid green line*) to the experimental data results in an exponential gain coefficient of $\Gamma \approx 18$ cm^{-1} for both waveguide and bulk

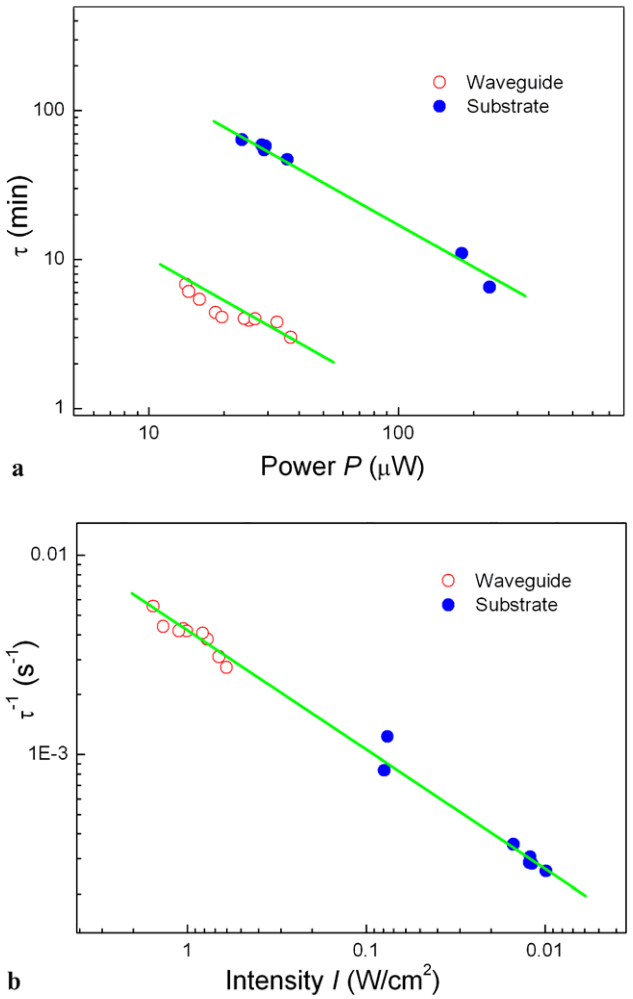

Fig. 6 Measured TWM response time τ versus total incident power P (**a**) and τ^{-1} versus intensity I (**b**) in both the waveguide (*open circles*) and the bulk (*filled circles*)

tal of ∼14% and assuming a coupling efficiency out of the waveguiding layer (due to defects on the crystal's endfacet) of ∼70%. For simplicity, the accuracy of the power values inside the sample is estimated to be about 20%, while power ratios are assumed to be accurate within 10%. To calculate the exponential gain factor Γ, also known as the TWM gain coefficient, we perform a numerical simulation of the experimental data, which was first raised by Fluck et al. for two-dimensional analysis of focused Gaussian beams [32]. As we can see, the waveguide and bulk possess almost the same properties. When the full intersection angle 2θ of the beams inside the waveguide is ∼16° (effective interaction length of the two beams is $L_{\text{eff}} \approx 1.3$ mm in this case), the best fit to the experimental data results in a gain of $\Gamma \approx 18\ \text{cm}^{-1}$.

Figures 6(a) and 6(b) depict the measured TWM response time τ evolution versus total incident power P and intensity I in both the waveguide and the bulk, respectively. For the latter, the cross section of the waveguide is 3 μm (obtained from the waveguide's index profile) times 800 μm (measured FWHM of lateral Gaussian intensity profile of the beam), leading to an area of $2.4 \times 10^{-3}\ \text{mm}^2$, while the respective cross section in the bulk is $0.27\ \text{mm}^2$. The relative errors of these cross sections are estimated to be about 20%. As one can see, at comparable total incident power, the built-up time of the induced gratings in the waveguide is reduced by more than one order of magnitude, with respect to that of the bulk. However, as shown in Fig. 6(b) where the inverse time constant τ^{-1} is plotted versus intensity I inside the sample, for the same intensity values the τ values are almost the same in the two regions. The inverse of the (Maxwell) time constant τ is proportional to the product of specific photoconductivity $\sigma_{\text{ph},0}$ and intensity I:

$$\tau^{-1} = \frac{\sigma_{\text{ph},0}}{\varepsilon_0 \varepsilon_{33}} I, \tag{3}$$

where ε_0 is the dielectric constant in vacuum and $\varepsilon_{33} = 32$ is the static dielectric constant for $LiNbO_3$. A linear fit to the complete set of experimental data (including both waveguide and substrate) yields the (specific) photoconductivity $\sigma_{\text{ph},0} = 1 \times 10^{-16}\ \text{mV}^{-2}$. Thus, within the accuracy limits of our measurements, we find the same value for both the implanted layer and the substrate. This observation is different from earlier results on PR waveguides in some other crystals, such as $KNbO_3$ [33], SBN [34], and $BaTiO_3$ [35, 36], where the TWM response times were reduced by one to three orders of magnitude (i.e., photoconductivity was increased), compared to the respective bulk values, for the same impinging light intensity. Thus, from our results it is reasonable to conclude that the PR properties of the $LiNbO_3$ bulk material are well-preserved in the waveguides and not altered due to the implantation process.

By comparing these measured parameters of O^{3+} ion-implanted $LiNbO_3$ waveguide with those in Ti-diffused or proton-exchanged waveguides, we can make the following conclusions: (1) oxygen implantation does not affect the PR properties (for example, by chemical oxidation/reduction of PR centers due to the implanted ions), and the waveguide has comparable PR features as Ti-indiffused samples (but does not show an increase of Fe^{2+} concentration as observed in the surface layer of Ti in-diffused $LiNbO_3$); (2) the O^{3+} ion implanted waveguide has higher PR sensitivity than (annealed) proton-exchanged waveguides, where the PR properties are strongly degraded also in annealed samples by the induced lattice disorder and an increase of dark conductivity [5]; (3) the low-loss oxygen-implanted waveguide has a relatively large refractive index change of $\Delta n_e \approx +0.0035$ and an almost rectangular index profile, leading to strong light confinement. The index increases is comparable to that obtained for annealed proton-exchanged guides (i.e., samples with α-phase where the electro-optic and PR properties are well preserved), but only slightly larger than those obtained for typical single-mode waveguides using Ti in-diffusion. However, in both latter cases, light confinement

is weaker (lower intensity for fixed optical power) due to the broader, diffusion-type Gaussian index profiles.

4 Conclusions

We report on, to our knowledge for the first time, the PR properties of an O^{3+} ion-implanted waveguide in a Fe:$LiNbO_3$ crystal. The implanted waveguide has low propagation losses of 0.5 dB/cm for TE polarized light, which is due to the non-leaky light confinement of the "well+barrier"-type refractive index distribution. Two-wave-mixing experiments reveal that the PR properties, in terms of exponential gain as well as build-up time of light-induced gratings, are well preserved in the waveguide.

Acknowledgements This work is supported by the National Natural Science Foundation of China (NSFC, Grant No. 10505013), and NSFC-RFBR (Project No. 10711120169). The authors thank H.J. Ma and R. Nie for performing the ion implantation and Q.M. Lu for polishing the samples.

References

1. P. Günter, J.-P. Huignard (eds.), *Photorefractive Materials and Their Applications*, vol. 2 (Springer, Berlin, 2007)
2. M.P. Petrov, S.I. Stepanov, A.V. Khomenko (eds.), *Photorefractive Crystals in Coherent Optical Systems* (Springer, Berlin, 1991)
3. K. Buse, Appl. Phys. B **64**, 1432 (1997)
4. S.E. Miller, Bell Syst. Tech. J. **48**, 2059 (1969)
5. D. Kip, Appl. Phys. B **67**, 131 (1998)
6. G.A. Torchia, A. Rodenas, A. Benayas, E. Cantelar, L. Roso, D. Jaque, Appl. Phys. Lett. **92**, 111103 (2008)
7. J.I. Mackenzie, IEEE J. Sel. Top. Quantum Electron. **13**, 626 (2007)
8. D. Fluck, P. Günter, IEEE J. Sel. Top. Quantum Electron. **6**, 122 (2000)
9. G. Keiser, *Optical Fiber Communications* (McGraw-Hill, Boston, 2000)
10. D. Kip, E. Krätzig, Opt. Lett. **17**, 1563 (1992)
11. D. Kip, M. Wesner, E. Krätzig, V.M. Shandarov, P. Moretti, Appl. Phys. Lett. **72**, 1960 (1998)
12. O. Matoba, K. Itoh, K. Kuroda, Proc. IEEE **87**, 2030 (1999)
13. J. Hukriede, D. Runde, D. Kip, J. Phys. D **36**, R1 (2003)
14. L. Arizmendi, Phys. Status Solidi A **2**, 253 (2004)
15. P. Zhang, D. Yang, J. Zhao, M. Wang, Opt. Eng. **45**, 074603 (2006)
16. L.W. Stultz, Appl. Opt. **18**, 2041 (1979)
17. D. Young, R.S. Feigelson, M.M. Fejer, M.F.J. Digonnet, H.J. Shaw, Opt. Lett. **16**, 995 (1991)
18. J.M. Cabrera, J. Olivares, M. Carrascosa, J. Rams, R. Müller, E. Dieguez, Adv. Phys. **45**, 349 (1996)
19. P.G. Suchoski, T.K. Findakly, F.J. Leonberger, Opt. Lett. **13**, 1050 (1988)
20. P.D. Townsend, P.J. Chandler, L. Zhang, *Optical Effects of Ion Implantation* (Cambridge University Press, Cambridge, 1994)
21. F. Chen, X.L. Wang, K.M. Wang, Opt. Mater. **29**, 1523 (2007)
22. S.M. Kostritskii, P. Moretti, J. Appl. Phys. **101**, 094109 (2007)
23. F. Chen, H. Hu, X.L. Wang, F. Lu, K.M. Wang, J. Appl. Phys. **98**, 044507 (2005)
24. G.G. Bentini, M. Bianconi, M. Chiarini, L. Correra, C. Sada, P. Mazzoldi, N. Argiolas, M. Bazzan, R. Guzzi, J. Appl. Phys. **92**, 6477 (2002)
25. J. Olivares, G. García, A. García-Navarro, F. Agulló-López, O. Caballero, A. García-Cabañes, Appl. Phys. Lett. **86**, 183501 (2005)
26. J. Rams, J. Olivares, P.J. Chandler, P.D. Townsend, J. Appl. Phys. **84**, 5180 (1998)
27. S.J. Field, D.C. Hanna, D.P. Shepherd, A.C. Tropper, P.J. Chandler, P.D. Townsend, L. Zhang, Opt. Lett. **16**, 481 (1991)
28. M.R. Beghoul, B. Fougere, A. Boudrioua, C. Darraud, S. Latreche, R. Kremer, P. Moretti, J.C. Vareille, Opt. Quantum Electron. **39**, 333 (2007)
29. A. Dazzi, P. Mathey, P. Lompré, P. Jullien, S.G. Odoulov, P. Moretti, J. Opt. Soc. Am. B **16**, 256 (1999)
30. P.K. Tien, R. Ulrich, R.J. Martin, Appl. Phys. Lett. **14**, 291 (1969)
31. P.J. Chandler, F.L. Lama, Opt. Acta **33**, 127 (1986)
32. D. Fluck, S. Brülisauer, P. Günter, Opt. Commun. **115**, 626 (1995)
33. S. Brülisauer, D. Fluck, P. Günter, L. Beckers, C. Buchal, J. Opt. Soc. Am. B **13**, 2544 (1996)
34. D. Kip, B. Kemper, I. Nee, R. Pankrath, P. Moretti, Appl. Phys. B **65**, 511 (1997)
35. A. Dazzi, P. Mathey, P. Lompré, P. Jullien, P. Moretti, D. Rytz, J. Opt. Soc. Am. B **16**, 1915 (1999)
36. K.E. Youden, S.W. James, R.W. Eason, P.J. Chandler, L. Zhang, P.D. Townsend, Opt. Lett. **17**, 1509 (1992)